analytical chemistry

Article

Cite This: *Anal. Chem.* 2020, 92, 2112−2120

pubs.acs.org/ac

Portable NMR with Parallelism

Ka-Meng Lei,[†,‡] Dongwan Ha,[‡] Yi-Qiao Song,[§] Robert M. Westervelt,[‡,∥] Rui Martins,[†,⊥] Pui-In Mak,*[,†] and Donhee Ham*[,‡]

[†]State Key Laboratory of Analog and Mixed-Signal VLSI, University of Macau, Macau, P. R. China

[‡]John A. Paulson School of Engineering and Applied Sciences, Harvard University, Cambridge, Massachusetts 02138, United States

[§]Schlumberger-Doll Research Center, Cambridge, Massachusetts 02139, United States

[∥]Department of Physics, Harvard University, Cambridge, Massachusetts 02138, United States

[⊥]Instituto Superior Técnico, Universidade de Lisboa, Lisbon 1049-001, Portugal

Supporting Information

ABSTRACT: Portable NMR combining a permanent magnet and a complementary metal-oxide-semiconductor (CMOS) integrated circuit has recently emerged to offer the long desired online, on-demand, or in situ NMR analysis of small molecules for chemistry and biology. Here we take this cutting-edge technology to the next level by introducing parallelism to a state-of-the-art portable NMR platform to accelerate its experimental throughput, where NMR is notorious for inherently low throughput. With multiple (N) samples inside a single magnet, we perform simultaneous NMR analyses using a single silicon electronic chip, going beyond the traditional single-sample-per-magnet paradigm. We execute the parallel analyses via either time-interleaving or magnetic resonance imaging (MRI). In the time-interleaving method, the N samples occupy N separate NMR coils: we connect these N NMR coils to the single silicon chip one after another and repeat these sequential NMR scans. This time-interleaving is an effective parallelization, given a long recovery time of a single NMR scan. To demonstrate this time-interleaved parallelism, we use N = 2 for high-resolution multidimensional spectroscopy such as J-coupling resolved free induction decay spectroscopy and correlation spectroscopy (COSY) with the field homogeneity carefully optimized (<0.16 ppm) and N = 4 for multidimensional relaxometry such as diffusion-edited T_2 mapping and T_1-T_2 correlation mapping, expediting the throughput by 2−4 times. In the MRI technique, the N samples (N = 18 in our demonstration) share 1 NMR coil connected to the single silicon chip and are imaged all at once multiple times, which reveals the relaxation time of all N samples simultaneously. This imaging-based approach accelerates the relaxation time measurement by 4.5 times, and it could be by 18 times if the signal-to-noise were not limited. Overall, this work demonstrates the first portable high-resolution multidimensional NMR with throughput-accelerating parallelism.

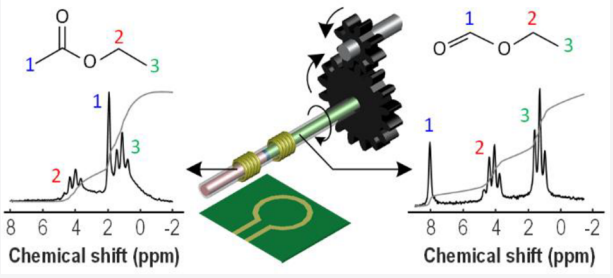

Nuclear magnetic resonance (NMR) is one of the most valuable analytical tools available to chemistry and biology. With its celebrated ability to elucidate the structure and function of the molecules at atomic resolution, NMR has revolutionized many branches of chemistry and beyond, such as organic chemistry, medicinal chemistry (drug discovery), structural biology, medical imaging, and oil exploration in the Earth's subsurface.[1−6]

One major thrust for further advancing this power of NMR has been to increase the field (B_0) of a superconducting magnet, with the state of the art[7−9] reaching 35 T, corresponding to a ^{1}H NMR frequency (f_0) of ∼1.5 GHz. The increased field enhances the signal-to-noise ratio (SNR) and also better resolves the complex spectral structures. Such bulky and heavy high-field instruments are well-suited for analyzing macromolecules (e.g., proteins) in structural biology, which is a frontier of the NMR science. Interestingly, another—and more recent—thrust for advancing the NMR instrumentation is quite the opposite of the above: it seeks miniaturization by replacing the superconducting magnet with a small permanent magnet with the field only on the order of 1 T. Such low-field systems cannot examine macromolecules, but with portability and low cost, they can be broadly distributed to perform cryogen-free online, on-demand, or in situ analyses of small molecules resulting from a wide variety of chemical and biochemical processes. The miniaturization is enabled by two recent advances: development of NMR-grade permanent magnets[10−13] and realization of NMR radio frequency (RF) electronics in complementary metal-oxide-semiconductor (CMOS) integrated circuits (ICs), also known as silicon electronic chips.[14−22] In fact, we recently combined CMOS ICs and permanent magnets to make the entire NMR platform portable for not only relaxation time measurements, or

Received: October 10, 2019
Accepted: December 18, 2019
Published: January 2, 2020

DOI: 10.1021/acs.analchem.9b04633
Anal. Chem. 2020, 92, 2112−2120

relaxometry,[16−20] but also fully pledged multidimensional NMR spectroscopy.[21,22]

One critical drawback of NMR, whether with superconducting or permanent magnets, is its inherently low throughput. A single NMR scan already takes several seconds. Moreover, to extract sufficient molecular information, a large number of such scans is often required, with two-dimensional (2D) NMR being a typical example. It can easily take over an hour to acquire a 2D NMR spectrum even for a small molecule. The theme of this work is to improve the throughput of portable NMR by exploiting parallelism. We analyze in parallel multiple samples placed in the same permanent magnet bore to boost the throughput, going beyond the traditional single-sample-per-magnet paradigm. Such multisample-per-magnet strategy has been explored with the superconducting magnet,[23−27] but never with a portable multidimensional high-resolution NMR platform. Recently multisample NMR with a permanent magnet[28] was reported, but it lacked 2D NMR capability as well as the resolution for fine spectral splitting such as *J*-coupling, both of which are essential for modern NMR; it also did not report integrated electronics.

We demonstrate the parallelism with our state-of-the-art portable NMR system[21] consisting of a permanent Halbach magnet (B_0 = 0.51 T; 7.3 kg) and a silicon spectrometer IC (Figure 1a). We configure this system in three ways to feature parallelism: (1) for 1D and 2D high-resolution spectroscopy we put 2 samples occupying 2 separate NMR coils in the magnet (Figure 1b); (2) for 1D and 2D relaxometry, we put 4 samples occupying 4 separate NMR coils in the magnet (Figure 1c); and (3) we develop a magnetic resonance imaging (MRI) configuration to simultaneously measure the relaxation time of 18 samples occupying 1 shared NMR coil (Figure 1d).

For the first and second configurations (Figures 1b,c), we connect the multiple coils to the single silicon chip in a time-interleaved fashion, exploiting the long recovery time of each NMR scan, hence effectively parallelizing NMR analysis (Figure 1e). This approach to parallelism increases the experimental throughput by 2−4 times. To place multiple samples in the same magnet, we should extend the region of an acceptable B_0-inhomogeneity in the magnet, a task especially critical for the first configuration aimed at high-resolution spectroscopy (Figure 1b): by using shim coils, which are designed to produce particular static magnetic field patterns upon current injection to compensate the magnet's field inhomogeneity, and also by rotating samples for motional averaging, we achieve $\Delta B_0/B_0$ (field inhomogeneity) < 0.16 ppm (3.5 Hz) across a sample volume of 0.8 μL, no matter where the sample is placed within a distance of ∼4.5 mm on the central axis of the magnet bore. The improved B_0-inhomogeneity allows placing 2 samples in the magnet (Figure 1b) to expedite by 2 times 1D and 2D spectroscopy such as free induction decay (FID) spectroscopy and correlation spectroscopy (COSY). For the second configuration aimed at relaxometry (Figure 1c), the field homogeneity requirement is not as stringent, and the Halbach magnet alone without shimming and motional averaging offers a sufficient homogeneity to accommodate up to 4 samples. This configuration accelerates by up to ∼4 times the 1D and 2D relaxometry, such as measuring spin−spin relaxation time (T_2), diffusion-edited T_2 measurements to distinguish molecular motion and nuclear spin relaxation, and correlating spin−lattice relaxation time (T_1) with T_2.

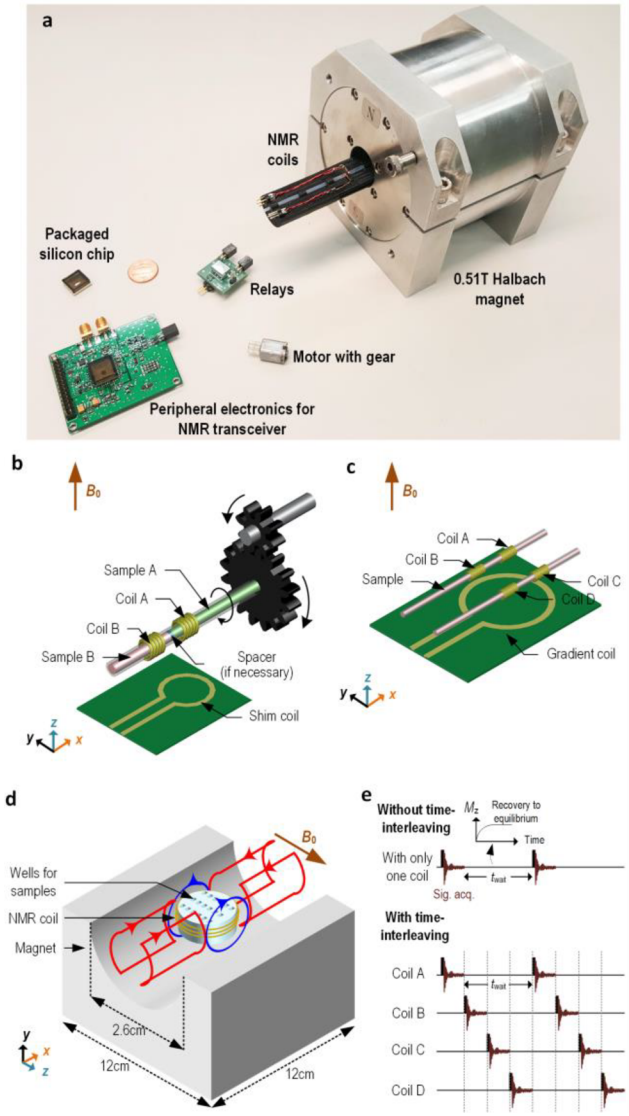

Figure 1. Portable NMR with parallelism. (a) Our portable NMR platform, whose key components are the Halbach magnet and the silicon IC we developed. (b) NMR spectroscopy configuration with 2 samples occupying 2 separate NMR coils. For field homogeneity optimization, it houses a rotational machinery and shim coils, whose illustration is simplified. (c) NMR relaxometry configuration with 4 samples occupying 4 separate NMR coils. It houses a gradient coil, whose illustration is simplified. (d) MRI configuration with 18 samples sharing 1 NMR coil. It also contains 2 sets of gradient coils for PE (red) and FE (blue), whose current directions are shown with the arrows on the gradient coil traces. (e) Time-interleaved operation to sequentially connect multiple coils to the single silicon chip for effective parallelization.

In the third configuration (Figure 1d), 1 NMR coil contains 18 samples and simultaneously measures the relaxation time of all 18 samples using the MRI technique. This arrangement can handle the larger number of samples because it is not limited by the interference among multiple samples/coils as in the first and second configurations. At the same time, since this setup has a lower filling factor and thus a lower SNR per sample, it is particularly useful for mass screening in non-SNR-limited applications. Our particular demonstration is the example where SNR is limited so the throughput is enhanced by 4.5 times despite the use of the 18 samples. But were it not for the

DOI: 10.1021/acs.analchem.9b04633
Anal. Chem. 2020, 92, 2112−2120

SNR limitation, the throughput would be increased by 18 times. This platform is also the first portable MRI, consisting of a permanent magnet and integrated electronics.

In summary, the 3 configurations firmly demonstrate portable multidimensional high-resolution NMR with parallelism for increased experimental throughput.

RESULTS AND DISCUSSIONS

Time-Interleaved Spectroscopy (Figure 1b Configuration with 2 Samples in 2 Separate NMR Coils). The Halbach magnet generates B_0 = 0.51 T (thus f_0 = 21.8 MHz) along the z-axis, while the magnet bore (length and diameter: ∼12 and 2.6 cm) lies along the x-axis (Figure 1). The magnet exhibits a field inhomogeneity down to 0.4 ppm over a sample volume of ∼0.8 μL (all field inhomogeneity reported in this subsection is over this volume) near the bore center, but the inhomogeneity increases sharply by 13−15 times (5−6 ppm) at ±2 mm away from the bore center along the x-axis. To house more than 1 sample for spectroscopy work, we must attain a sub-ppm resolution across a region far beyond the inherent sweet spot. To this end, we use both miniaturized shim coils[29] and motional averaging: to resolve J-coupling of the alkyl group, which is typically ∼7 Hz, or ∼0.32 ppm for f_0 = 21.8 MHz, we target $\Delta B_0/B_0 \approx 0.16$ ppm (half of J-coupling) across several mm along the x-axis with the shimming and motional averaging.

$\Delta B_0/B_0$ is inferred from the measured line width Δf_0 of the water ^{1}H FID using $\Delta f_0 = \gamma \Delta B_0/2\pi$ (γ: proton gyromagnetic ratio). We move a standard PTFE tube containing the sample, a surrounding NMR coil, and shim coils altogether within the distance of ∼± 2.5 mm about the bore center along the x-axis with an increment of 0.5 mm and measure the ^{1}H FID spectrum at the 11 resulting positions. $\Delta B_0/B_0$ measured at these positions are in Figure 2a. With only the shim coils with no rotation (red, Figure 2a), the inhomogeneity is reduced to below 0.4 ppm across the 5 mm distance, with the best value reaching 0.17 ppm near the bore center. This is a substantial improvement from the inhomogeneity as high as 5−6 ppm with no shimming. Yet to further the homogeneity to resolve J-coupling, we rotate the sample about the x-axis, which is the well-known motional averaging[30,31] yet has not been used in portable NMR. Figure 2a, the blue shows the $\Delta B_0/B_0$ with the rotational frequency, f_R, of 40 Hz, where the 0.16 ppm target is met within −2 mm and +2.5 mm from the bore center along the x-axis. This level of homogeneity allows placing more than 1 sample in the magnet bore. The sample is rotated by turning the tube using a small DC motor and gears (Supporting Information, SI, Note S1 and Figure S1).

f_R = 40 Hz (2,400 rpm) is selected on the following ground. For the rotation to effectively average out the field inhomogeneity, f_R must exceed the line width due to the field inhomogeneity,[30] that is, $f_R > \gamma \Delta B_0/2\pi$ must be satisfied. Since $\Delta B_0/B_0$ with the shim coils only is as large as ∼0.4 ppm, f_R > 8.7 Hz should be met (to be rigorous, this statement is most accurate if the ∼0.4 ppm inhomogeneity were purely along the y- and z-directions; in reality, inhomogeneity exists along the x-direction as well, which cannot be removed by the rotation about the x-axis). The measured ^{1}H FID spectrum shows a clear line width reduction with $f_R \geq 10$ Hz (Figure 2b). We choose a high enough f_R of 40 Hz to avoid any appreciable sidebands.

With the expanded region satisfying $\Delta B_0/B_0 \approx 0.16$ ppm over the 4.5 mm distance along the bore's central axis, we could densely line up 5 samples with 5 NMR coils (length: 0.8 mm each, SI Note S2), but we instead place 2 samples with 2 NMR coils along the central axis, sharing the same PTFE tube (OD: 1.7 mm; ID: 1 mm), with a sample-to-sample (center-to-center) separation of 3 mm (Figure 1b). This separation is to minimize the undesired coupling of an NMR coil with the sample in the neighboring NMR coil. The 3 mm separation is determined from a finite element analysis of RF magnetic field of an NMR coil (COMSOL Multiphysics; Figure S2). When the 2 samples are of different types, we place a spacer between them by modifying the tube (SI Note S3). The shim coils (not to be confused with NMR coils) for the 2 samples are fabricated on the same printed circuit board (PCB), and two identical such PCBs are placed at the bottom (Figure 1b) and the top (not shown in Figure 1b) in the magnet, sandwiching the samples, to correct the B_0-inhomogeneities for all directions at both sample regions. Figure S3 shows the detailed construction of these shim coils. The ^{1}H FID spectra from 2 water samples are juxtaposed in Figure 2c; both attain a line width less than 0.16 ppm. A brief description of the NMR data processing can be found in SI Note S4.

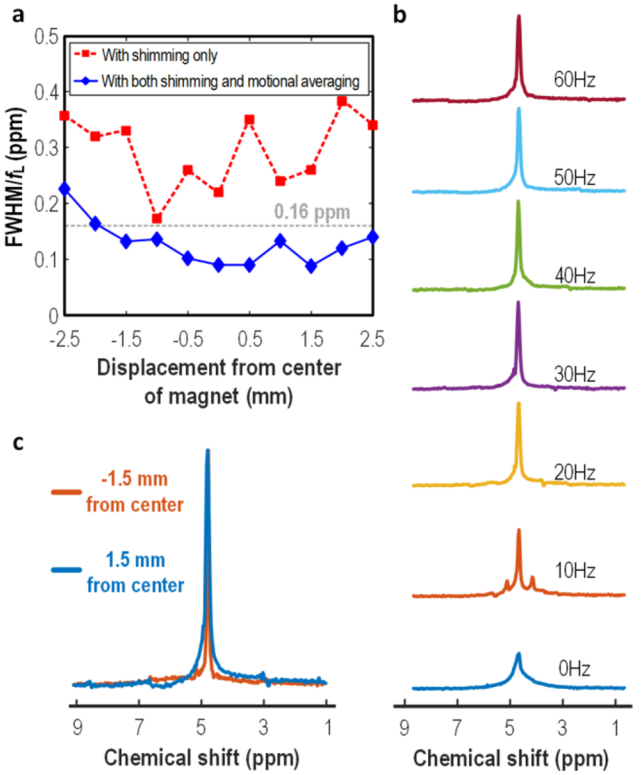

Figure 2. Line width narrowing across the magnet bore via shimming and motional averaging. (a) Measured line widths of the water ^{1}H FID spectra at different locations from the center of the Halbach magnet bore along the x-axis. Without shim coils and motional averaging, the line width (thus the field inhomogeneity) is as high as 5−6 ppm (not shown) at ±2 mm away from the bore center along the x-axis. The shim coil brings the line width down to below 0.4 ppm across the 5 mm distance along the x-axis. The 40-Hz rotation in addition further improves the line width below 0.16 ppm for the majority of tested positions. (b) The water ^{1}H FID spectra with varying rotation frequencies at 1.5 mm along the x-axis from the magnet center. Sidebands appear with rotation frequencies below 20 Hz. (c) The water ^{1}H FID spectra at +1.5 mm and −1.5 mm from the center along the x-axis with the 40-Hz rotation and the shim coils.

DOI: 10.1021/acs.analchem.9b04633
Anal. Chem. 2020, 92, 2112−2120

The parallel analysis of the 2 samples is done with time-interleaving, which we explain here generally with N samples occupying N separate NMR coils (N = 2 in this subsection; N = 4 in the next; N = 4 in Figure 1e). We connect the N NMR coils to the single silicon IC one after another to perform a single NMR scan for each sample sequentially. We repeat this sequence, if multiple scans for each sample are necessary. Since a single scan for a sample is followed by a long recovery time ($\sim 5T_1$) of several seconds before the next scan can be performed on that sample, within the recovery time of 1 sample, the sequential $N-1$ scans for the remaining $N-1$ samples can be finished (unless N is excessively large). Thus, the time-interleaving effectively parallelizes NMR analyses.

This 2-sample/2-NMR-coil spectroscopy (Figure 1b) is first validated by measuring 1D ^{1}H FID spectra of 2 samples of the identical type (Figure 3a), ethyl formate ($C_3H_6O_2$). Each coil executes 8 scans (2 sets of 4-step phase cycling), so in total 16 scans are performed by the 2 coils in the time-interleaved manner (Figure S4a). The resulting spectra are aligned and summed to increase the SNR. The total data acquisition time of ~52 s is halved from the case of performing 16 sequential scans on a single sample. The final spectrum (Figure 3a) resolves not only the chemical shifts of 1.3, 4.2, and 8.0 ppm for CH_3, CH_2, and OH groups but also 4 and 3 fine-split peaks in CH_2 and CH_3 groups that correctly show J-couplings (~7 Hz), attesting to our resolution (0.16 ppm or ~3 Hz). In Figure 3b, we measure 2 samples of distinct types, ethyl formate and ethyl acetate ($C_4H_8O_2$). Each coil executes 16 FID scans, with a total data acquisition time of ~107 s with time-interleaving, an acceleration by 2 times. All chemical shifts and J-couplings (~7 Hz) are resolved. If we turn off motional averaging, then chemical shifts are still resolved but J-coupled multiplets disappear (Figure S4b), confirming the role of motional averaging in achieving $\Delta B_0/B_0$ < 0.16 ppm across both sample regions.

One highlight of our system capabilities is parallelized 2D spectroscopy, which we demonstrate by performing COSY simultaneously on ethyl formate and ethyl acetate (Figure 4).

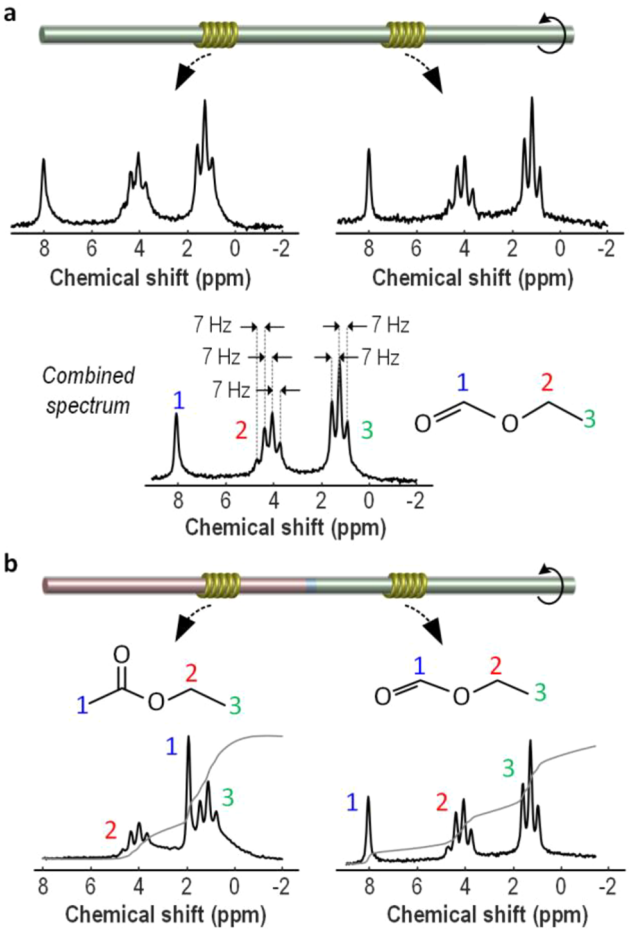

Figure 3. Measured 1D ^{1}H NMR spectra with time-interleaving (2 NMR samples with 2 coils). (a) Measured 1D ^{1}H spectra of 2 samples of the identical content (ethyl formate). Eight FID scans from each sample are time-interleaved, shortening the total data acquisition time to ~52 s. (b) Measured 1D ^{1}H spectra of 2 samples of differing contents (ethyl acetate and ethyl formate).

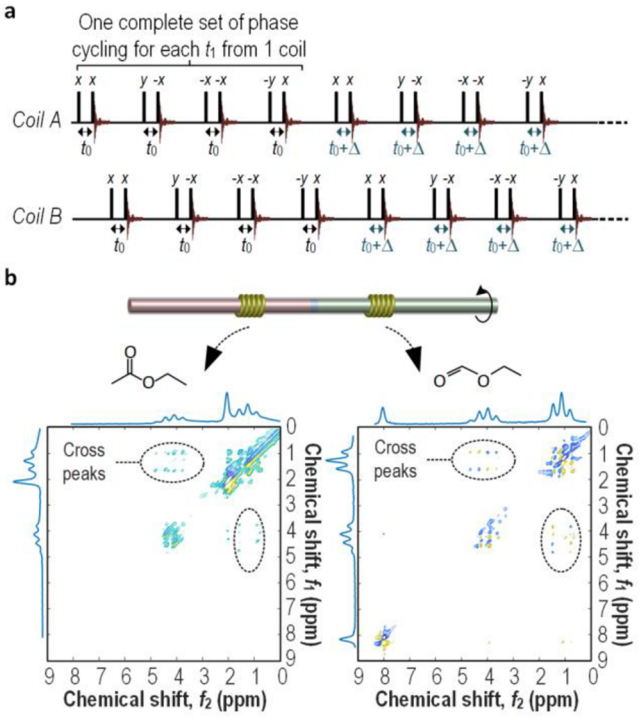

Figure 4. Measured 2D ^{1}H NMR spectra with time-interleaving (2 NMR samples with 2 coils). (a) Time-interleaved COSY scans for 2 samples of differing contents (ethyl formate and ethyl acetate). Each sample undergoes 404 total scans. (b) Measured COSY spectra of ethyl formate and ethyl acetate.

Figure 4a shows COSY pulse sequences—including phase cycling—applied to the 2 NMR coils. They are time-interleaved exploiting the long recovery between two neighboring scans in each sequence. The two COSY experiments are done effectively in parallel within 48 min, which would otherwise take twice longer. The cross peaks, a primary interest in COSY, are well resolved in either spectrum (Figure 4b) due to the resolution of the platform with the shimming and motional averaging, while the latter tends to distort the diagonal peaks.

Time-Interleaved Relaxometry (Figure 1c Configuration with 4 Samples in 4 Separate NMR Coils). For relaxometry B_0-homogeneity requirement is relaxed, and we use neither shim coils nor motional averaging. Moreover, we load 4 samples with 4 NMR coils in 2 tubes, where the 2 tubes are separated by 4 mm, and the 2 samples in either tube are

DOI: 10.1021/acs.analchem.9b04633
Anal. Chem. 2020, 92, 2112−2120

separated by 4 mm (Figures 1c and S1). To measure molecular diffusion along with NMR relaxation time, we use a gradient coil that generates a B_0-gradient of 0.11 T/m in the z-direction (Figures 1c and S5a,b). In all relaxometry experiments we present (Figures 5, S6, and S7), the 4 samples are of identical type, although 4 different types of samples can also be analyzed in parallel.

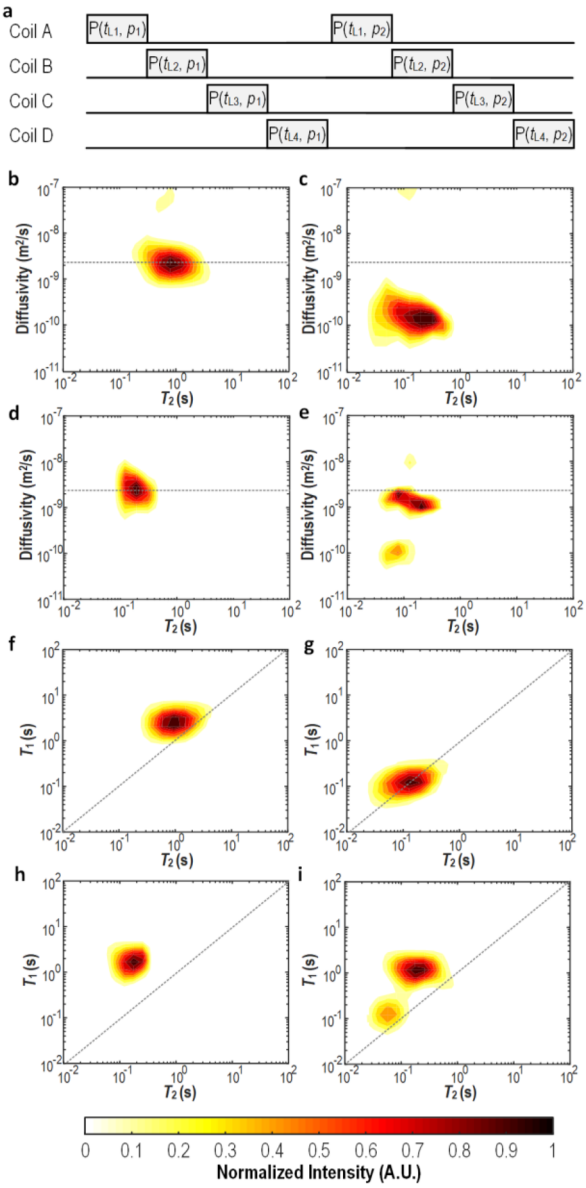

Figure 5. 2D $D-T_2$ and T_1-T_2 maps of the samples with time-interleaving (4 NMR samples with 4 coils). (a) Time-interleaved distribution of the modified CPMG pulse sequences across 4 samples of the identical type for $D-T_2$ mapping acceleration. $P(t_{Li}, p_j)$ represents a single scan sequence where t_{Li} is an i-th long echo spacing value ($i = 1 \sim n$) and p_j indicates the j-th phase cycling ($j = 1-4$). (b–e) 2D $D-T_2$ maps of deionized water (acquisition time: 2.1 min, 80 scans), light oil (2.3 min, 80 scans), skim milk (2.1 min, 80 scans), and heavy cream (6.5 min, 256 scans). The diffusivity of water at room temperature (2.2×10^{-9} m^2/s) is marked with the dashed lines. (f–i) 2D T_1-T_2 maps of deionized water (acquisition time: 9.1 min, 80 scans), light oil (4.0 min, 80 scans), skim milk (6.7 min, 80 scans), and heavy cream (14.7 min, 256 scans). The dashed diagonal lines are for $T_1 = T_2$.

First, we perform 2D diffusion-edited NMR relaxometry with the gradient coil activated to obtain the map of the diffusivity D of ^{1}H containing molecules[32,33] vs T_2, which tells apart the effect of molecular diffusion from the pure spin–spin relaxation, a strategy useful in the food industry,[34] well-logging,[35] and geophysical study.[33] This analysis entails a large number of NMR scans. Each scan uses a modified Carr–Purcell–Meiboom–Gill (CPMG) pulse sequence: the first 2 echoes have a long spacing of t_L, followed by a subsequent pulse train of short echo spacing (t_S). As ^{1}H-containing molecules appreciably diffuse during t_L, the ^{1}H spins experience a considerable B_0 gradient, and thus the echo amplitude right after t_L is reduced by more than that which T_2 relaxation predicts: this extra reduction bears information on how fast the diffusion becomes. In contrast, during the short echo spacing t_S, no significant diffusion occurs and hence the echo amplitude reduction corresponds to the T_2 relaxation. Through different scans, t_L is varied while t_S is fixed so that the $D-T_2$ map can be constructed. For n different t_L values, the total number of scans is $4n$ with 4-step phase cycling. We distribute and parallelize these $4n$ scans across 4 samples of the identical content in the time-interleaved manner to expedite the experiment by 4 times (Figure 5a). Each sample undergoes n scans with its own *exclusive* set of t_L values and corresponding 4-step phase cycling (n is chosen as a multiple of 4). The results from the 4 identical types of samples with the mutually exclusive set of t_L values are then collected and processed to construct the $D-T_2$ map (SI Note S4 and Figure S6).

Figure 5b–e shows the so-obtained $D-T_2$ maps for deionized water, light oil, skim milk, and heavy cream. n = 20 for Figure 5b–d, while n = 64 for Figure 5e. t_S is fixed at 0.6 ms for all scans. The $D-T_2$ map of deionized water (Figure 5b) reveals $D \approx 2.2 \times 10^{-9}$ m^2/s and $T_2 \approx 1$ s, which are consistent with the well-established data. The light oil (Figure 5c) shows a lower T_2 (~100 ms) and a lower D ($\sim 1.3 \times 10^{-10}$ m^2/s), for the viscosity is higher in light oil ($\lesssim$30 cP) than in water (~1 cP). Figures 5d and 5e for skim milk and heavy cream reveal the power of this 2D relaxometry to tell apart the two distinct materials: while skim milk (no fat) shows a single peak at $T_2 \approx 200$ ms and $D \approx 2.2 \times 10^{-9}$ m^2/s for its water content (Figure 5d), the heavy cream (36% fat) shows two appreciable peaks with one at $T_2 \approx 130$ ms and $D \approx 1.3 \times 10^{-9}$ m^2/s for its water content and the other at $T_2 \approx 100$ ms and $D \approx 1 \times 10^{-10}$ m^2/s for its liquid fat content (Figure 5e). The total data acquisition time, for example in the case of the heavy cream (Figure 5e), is 6.5 min, while it would have taken 26 min in the absence of parallelism.

We perform another 2D relaxometry, the T_1-T_2 mapping, where each scan consists of an inversion recovery sequence followed by a CPMG pulse sequence (echo spacing: 0.6 ms).[32,34] Different scans are given different inversion times. By distributing multiple scans across the 4 samples of identical content just like in the $D-T_2$ mapping, we expedite the T_1-T_2 correlation mapping. Figure 5f–i shows the T_1-T_2 correlation maps for water, light oil, skim milk, and heavy cream. While the first 3 samples show a single peak, the last sample, heavy cream, shows 2 distinct peaks due to the water and fat contents. As the inversion time for a scan can be on the same order of magnitude as T_1, we cannot always pack 4 scans for the 4 samples within the recovery time. So the time-interleaving here is not as effective as those of all other experiments presented, but we still expedite by a factor larger than 2: the analysis of skim milk of Figure 5h, for example,

DOI: 10.1021/acs.analchem.9b04633
Anal. Chem. 2020, 92, 2112–2120

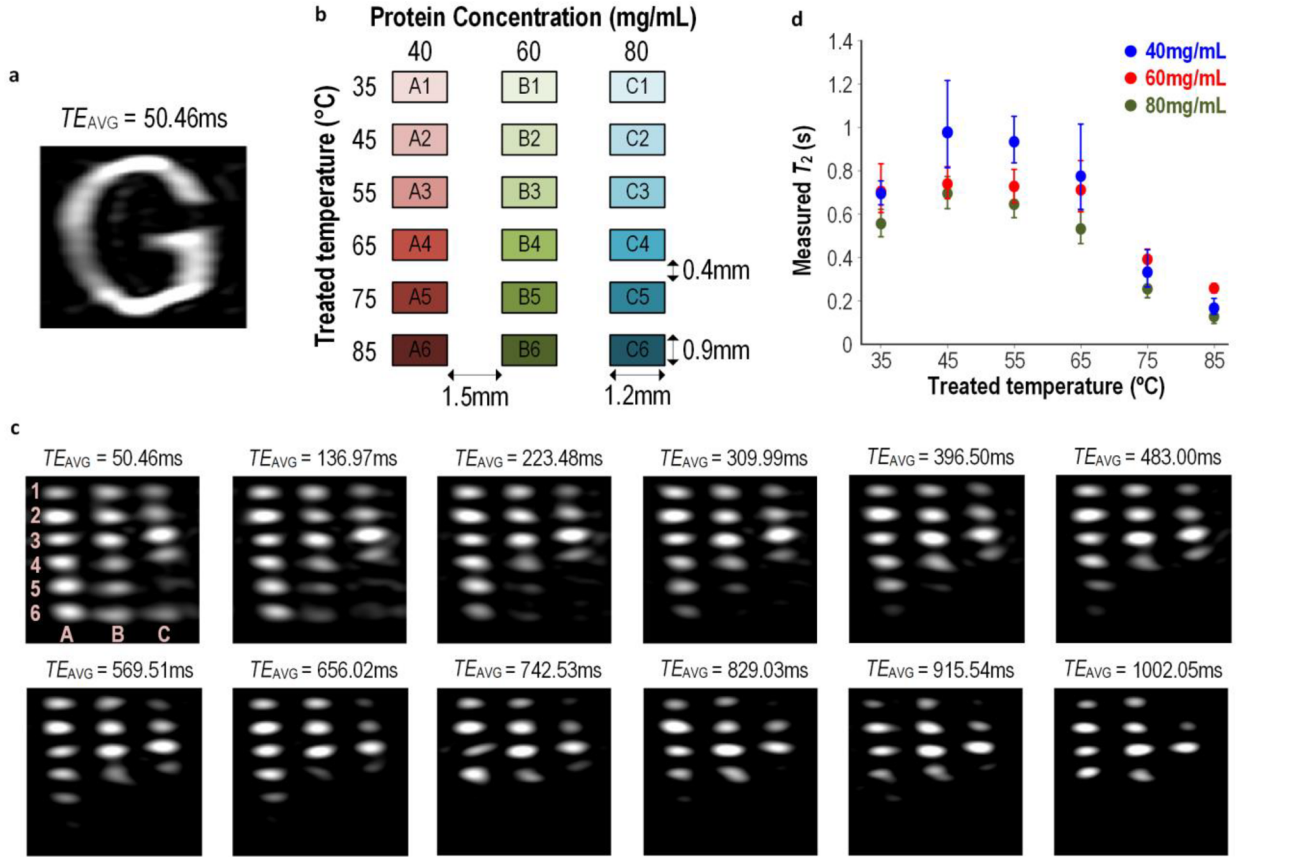

Figure 6. MRI for high-throughput T_2-screening (18 samples sharing 1 coil). (a) The acquired MRI image of the deionized water along the "*G*" trace engraved on an acrylic substrate with $TE_{AVG} \approx 50$ ms. (b) The 6 × 3 sample wells (~1.5 μL each) used for the high throughput T_2 screening. Protein β-lactoglobulin treated at 6 different temperatures at 3 different concentrations load these wells. (c) The acquired MRI images with different values of TE_{AVG}. All samples are clearly imaged with the smallest TE_{AVG} but their intensities tend to decrease gradually as TE_{AVG} increases, from which T_2 of each sample is extracted. (d) The measured T_2 of the 18 β-lactoglobulin samples.

takes 6.7 min to finish, while it would take ca. 15 min in the absence of the parallelism. This T_1-T_2 correlation mapping is also useful in increasing the confidence level of magnetic-particle-based biomolecular sensing,[36−38] and our platform accelerates such biomolecular sensing modality through parallelism, whose details we discuss in SI Note S5 and Figure S7.

Mass Screening (Figure 1d Configuration with 18 Samples Sharing 1 NMR Coil). In the foregoing *N* sample/*N* NMR coil strategy (Figure 1b and c), the sample number *N* was limited to 2−4 because coils should be sufficiently separated to minimize spurious coupling (also since the *N* NMR coils share the single silicon IC, we resorted to the time-interleaving technique). In contrast, in the *N* sample/1 NMR coil configuration of Figure 1d where the relaxation times of the *N* samples are measured all at once by the MRI technique, increasing the number of samples, *N*, is not limited by the cross-coil/sample interference, and our demonstration uses *N* = 18 (also the 1 NMR coil is always connected to the single silicon IC without needing the time-interleaving method). This *N* sample/1 NMR coil MRI configuration, however, has a lower filling factor thus a lower SNR per sample, so it is particularly useful for mass screening in non-SNR-limited applications, in which case the throughput can be increased by *N* times.

This MRI configuration of Figure 1d also features, inside the Halbach magnet, 2 sets of gradient coils for frequency encoding (FE) and phase encoding (PE) for ^{1}H spins. These gradient coils, which are of the Golay (for PE) and Maxwell (for FE) geometry (Figures 1d and S8; SI Note S6), generate the B_0-gradients along the *x*- and *z*-axis. Since we seek to acquire only 2D images on the $x-z$ plane, we do not implement the slice-selective scheme. The gradient coils for PE and FE are operated by a field-programmable-gate-array (FPGA) (Figure S9a) to precisely control the timing of the FE and PE B_0-gradient pulses in reference to the turbo spin echo[39] NMR scan performed by the silicon IC (Figure S9b,c). A single turbo spin echo scan can use a number of different acquisition time parameter (TE_{AVG}) values after an initial 90°-pulse to produce the same number of images in time sequence (Figure S10a), which show the decaying patterns of the NMR signals in the imaged area (8 PE steps, each with 40 digitized data points, are run together in attaining each image; the conjugate symmetry in the *k*-space[40] economizes the data acquisition). The signal decay of a specific region on the images reveals the T_2 of the sample in that region. Before we discuss the results with *N* = 18 samples, Figure 6a shows the acquired single image of the letter "*G*" (~9 mm in diameter) with the turbo spin echo using only one TE_{AVG} value (50 ms). The letter "*G*" is engraved on an acrylic substrate (trench depth: 2 mm) with a laser printer and filled with deionized water for ^{1}H NMR (Figure S10b). This image acquisition involving 4-step phase cycling and the intermittent spin recovery times takes ~20 s.

DOI: 10.1021/acs.analchem.9b04633
Anal. Chem. 2020, 92, 2112−2120

For the high-throughput screening with $N = 18$ with Figure 1d configuration, we engrave 6 × 3 wells (1.5 μL per well) on an acrylic substrate using the laser printer and fill them with β-lactoglobulin solutions (Figure 6b). The β-lactoglobulin molecules denature and aggregate when heated above 70 °C. This change alters the proton exchange process between the protein and the water molecule and thus influences the T_2 of the samples.[41,42] We prepare β-lactoglobulin at 3 concentrations (40, 60, and 80 mg/mL), and treat them in water bath at 6 temperatures (between 35 and 85 °C). These 18 distinct preparations load the 6 × 3 wells. One turbo spin echo scan containing 12 different values of TE_{AVG} produces 12 images. A total of 16 turbo spin echo scans are performed for 4-step phase cycling and also to improve the SNR, with the entire experiment taking ∼1.8 min. Figure 6c shows the resulting 12 images of the 6 × 3 sample wells. All 18 samples are clearly imaged with the smallest TE_{AVG}, whereas their image intensities decrease at different rates as TE_{AVG} increases, from which T_2 of each sample is extracted (Figure S11). Samples treated above 70 °C in wells A5, A6, B5, B6, C5, and C6 show significantly smaller T_2, as expected (Figure 6d). The parallel measurements of 18 samples accelerate the experiment by 4.5 times compared to the case without parallelism (1 sample/1 NMR coil situation with the full filling factor), where we do not obtain the full 18 times acceleration because this example is limited in the SNR requiring 4 scans for averaging for each phase cycling step. Yet 4.5 times acceleration in time is still substantial.

CONCLUSIONS

We have advanced the recently emerged portable multidimensional NMR technology to the next level by increasing its experimental throughput via a multisample-per-magnet parallelism strategy. On the one hand, we have performed time-interleaved NMR scans of 2−4 samples using 2−4 NMR coils with 1 silicon electronic chip for effectively parallel execution of multidimensional ^{1}H NMR spectroscopy (e.g., 1D FID and 2D COSY) and multidimensional ^{1}H NMR relaxometry (e.g., T_1−T_2 mapping and D−T_2 mapping). On the other hand, we have also demonstrated an MRI-based mass screening of 18 samples with 1 NMR coil and 1 silicon electronic chip, measuring their T_2 times with bona fide simultaneity. This work, especially the high-resolution spectroscopy, has also entailed the careful engineering of the magnetic field homogeneity to achieve <0.16 ppm over an extended region via shimming and motional averaging.

For the time-interleaving technique, the further increase of the sample number from 2−4 has been prevented. This is because, despite the substantial expansion of the region of the sub-ppm field homogeneity by shimming and motional averaging, the prevention of the coupling of an NMR coil with its neighboring sample requires an appreciable separation between NMR coils. This issue can be addressed in the future by further expanding the region of the sub-ppm field homogeneity, by decreasing the size of the NMR coils and samples, or by more misaligned (as opposed to colinear) arrangement of the samples using microfluidics. If the sample number is substantially increased in this way, then we can also consider using multiple silicon electronic chips inside the magnet to relax the number of the samples one silicon chip has to deal with. Since the silicon electronic chip is much smaller in volume than the sample we have used in our work, such parallelism with in-magnet electronics is a definite possibility and may enable the next generation of high-throughput portable NMR systems and advance the capability of NMR for chemistry.

In the MRI-based parallelization, the sample number (18) has been limited by the shape of the Halbach magnet bore: the bore shape constrains the possible geometry of the gradient coils, which in turn limits the linearity of the B_0-gradients. Consequently, the field-of-view for the imaging, and thus the number of samples that can be imaged, are limited. A possible improvement will be to adopt a magnet with an open bore design, such as the single-sided magnet,[10,11] which can give a far greater degree of freedom in choosing the geometry of the gradient coils, improving the linearity of the field gradient, thus increasing the field-of-view and the number of samples that can be measured simultaneously. In addition, various other parallel acquisition techniques developed for the standard bulky MRI systems[43,44] may be applied to this portable MRI platform to further optimize the data acquisition time.

METHODS AND MATERIALS

Electronics. The silicon IC packaged in a 48-pin ceramic chip carrier is placed on a 6-metal-layer PCB along with other peripheral electronics such as voltage regulators and analog-to-digital converter (ADC). Mechanical relays are used as switches between NMR coils and the silicon IC in time-interleaving (Figure S1b). A microcontroller board Cerebot MX7CK from Digilent (Pullman, WA) coordinates the PCB electronics (Figure S1). For the electronics for the MRI gradient-coils, see SI Note S7 and Figure S9.

Gradient Coils. The gradient coil for the time-interleaved relaxometry (Figure 1c) is of the Maxwell geometry,[45] consisting of two parallel planar subcoils implemented in two separate PCBs, which are placed in the magnet bore perpendicular to the z-direction, sandwiching the samples. Each subcoil on each PCB with 2 metal layers has 8 turns (4 turns on each metal layer). Each metal layer in the PCB is a 70 μm thick copper, which can support a large current to create a sufficient B_0-gradient. The width and spacing of the copper traces forming each subcoil are 0.39 mm and 0.15 mm, respectively. The 13 mm separation between the two PCBs is $\sqrt{3}$ times larger than the subcoil's average radius, 7.5 mm (Figure S5a). This Maxwell coil creates a nearly constant gradient across the sample (variation of the B_0-gradient across the sample <3%) at each of the 4 sensing spots (Figure S5b).

For the MRI system (Figure 1d), the Maxwell coil for FE is wound with 28 AWG enameled copper wire from Remington Industries (Johnsburg, IL). With 8 turns on each subcoil, it is oriented to create a B_0-gradient along the z-axis (Figure S8a). The separation between the two subcoils is $\sqrt{3}$ times larger than either subcoil's radius. The Golay coil for PE is also wound with 28 AWG enameled copper. With 8 turns on each subcoil, it is oriented to create a B_0-gradient along the x-axis (Figure S8d). Its geometry is optimized in COMSOL, with the B_0-gradient along the x-axis deviating by less than 10% across the field-of-view.

Materials. The biotin-labeled magnetic nanoparticles from Nanocs Inc. (Boston, MA) are diluted to designated concentrations with deionized water. All other samples are from Sigma-Aldrich (St. Louis, MO).

DOI: 10.1021/acs.analchem.9b04633
Anal. Chem. 2020, 92, 2112−2120

■ ASSOCIATED CONTENT

Supporting Information

The Supporting Information is available free of charge at https://pubs.acs.org/doi/10.1021/acs.analchem.9b04633.

Implementation of sample rotation; NMR/MRI coils; customized tube for two samples of different types; NMR data processing; magnetic-particle-based biomolecular sensing with parallelism; design of the gradient coils for MRI system; electronics for the gradient coils of MRI system; block diagrams of the proposed NMR spectrometer and relaxometer with parallelism; simulated magnetic-field pattern of the NMR coil; layout of the shim coils fabricated on PCB for 2 NMR samples; time-interleaved 1D ^{1}H NMR spectroscopic experiment; the gradient-coil for relaxometry; measured diffusion-edited NMR relaxation data of skim milk; relaxation rates measurement from avidin samples with the NMR relaxometer; design and simulation of the MRI gradient-coils; the hardware for the portable MRI; the MRI experiment on the phantom; and original data for the high-throughput T_2-screening with MRI (PDF)

■ AUTHOR INFORMATION

Corresponding Authors

*E-mail: pimak@um.edu.mo.

*E-mail: donhee@seas.harvard.edu.

ORCID

Ka-Meng Lei: 0000-0003-1781-971X

Donhee Ham: 0000-0001-6925-2466

Notes

The authors declare no competing financial interest.

■ ACKNOWLEDGMENTS

We thank Dr. Isik Kizilyalli, program director of the Advanced Research Projects Agency-Energy (ARPA-E), for the support of this research under contract DE-AR0001063. We also acknowledge the support of this work by the Macao Science and Technology Development (FDCT)—State Key Lab (SKL) Fund, Department of Energy Basic Energy Sciences grant (DE-FG02-07ER46422), and the National Science Foundation (DMR-1231319 and EFMA-1542807). Fabrication of the experimental components was partly done at the Center for Nanoscale Systems at Harvard University, which is supported by the National Science Foundation award no. 1541959.

■ REFERENCES

(1) Mittermaier, A.; Kay, L. E. *Science* **2006**, *312* (5771), 224−228.

(2) Liu, Y.; Sauri, J.; Mevers, E.; Peczuh, M. W.; Hiemstra, H.; Clardy, J.; Martin, G. E.; Williamson, R. T. Unequivocal determination of complex molecular structures using anisotropic NMR measurements. *Science* **2017**, *356* (6333), eaam5349.

(3) Inomata, K.; Ohno, A.; Tochio, H.; Isogai, S.; Tenno, T.; Nakase, I.; Takeuchi, T.; Futaki, S.; Ito, Y.; Hiroaki, H.; Shirakawa, M. *Nature* **2009**, *458*, 106−109.

(4) Sakakibara, D.; Sasaki, A.; Ikeya, T.; Hamatsu, J.; Hanashima, T.; Mishima, M.; Yoshimasu, M.; Hayashi, N.; Mikawa, T.; Wälchli, M.; Smith, B. O.; Shirakawa, M.; Güntert, P.; Ito, Y. *Nature* **2009**, *458*, 102−105.

(5) Puig-Castellvi, F.; Pérez, Y.; Piña, B.; Tauler, R.; Alfonso, I. *Anal. Chem.* **2018**, *90* (21), 12422−12430.

(6) Paudel, L.; Nagana Gowda, G. A.; Raftery, D. *Anal. Chem.* **2019**, *91* (11), 7373−7378.

(7) Bhattacharya, A. *Nature* **2010**, *463*, 605−606.

(8) Hashi, K.; Ohki, S.; Matsumoto, S.; Nishijima, G.; Goto, A.; Deguchi, K.; Yamada, K.; Noguchi, T.; Sakai, S.; Takahashi, M.; Yanagisawa, Y.; Iguchi, S.; Yamazaki, T.; Maeda, H.; Tanaka, R.; Nemoto, T.; Suematsu, H.; Miki, T.; Saito, K.; Shimizu, T. *J. Magn. Reson.* **2015**, *256*, 30−33.

(9) Gan, Z.; Hung, I.; Wang, X.; Paulino, J.; Wu, G.; Litvak, I. M.; Gor'kov, P. L.; Brey, W. W.; Lendi, P.; Schiano, J. L.; Bird, M. D.; Dixon, I. R.; Toth, J.; Boebinger, G. S.; Cross, T. A. *J. Magn. Reson.* **2017**, *284*, 125−136.

(10) Perlo, J.; Casanova, F.; Blümich, B. *Science* **2007**, *315* (5815), 1110−1112.

(11) Perlo, J.; Demas, V.; Casanova, F.; Meriles, C. A.; Reimer, J.; Pines, A.; Blümich, B. *Science* **2005**, *308* (5726), 1279.

(12) Hugon, C.; D'Amico, F.; Aubert, G.; Sakellariou, D. *J. Magn. Reson.* **2010**, *205* (1), 75−85.

(13) Magritek. Spinsolve 80 website, https://go.magritek.com/spinsolve-80-benchtop-nmr-brochure.

(14) Grisi, M.; Gualco, G.; Boero, G. A broadband single-chip transceiver for multi-nuclear NMR probes. *Rev. Sci. Instrum.* **2015**, *86* (4), 044703.

(15) Kim, J.; Hammer, B.; Harjani, R. *Proc. IEEE 2012 Custom Integrated Circuits Conf.* **2012**, 1−4.

(16) Lei, K.-M.; Heidari, H.; Mak, P.-I.; Law, M.-K.; Maloberti, F.; Martins, R. P. *IEEE J. Solid-State Circuits* **2017**, *52* (1), 284−297.

(17) Lei, K.-M.; Mak, P.-I.; Law, M.-K.; Martins, R. P. *IEEE J. Solid-State Circuits* **2016**, *51* (10), 2274−2286.

(18) Sun, N.; Liu, Y.; Lee, H.; Weissleder, R.; Ham, D. *IEEE J. Solid-State Circuits* **2009**, *44* (5), 1629−1643.

(19) Sun, N.; Yoon, T. J.; Lee, H.; Andress, W.; Weissleder, R.; Ham, D. *IEEE J. Solid-State Circuits* **2011**, *46* (1), 342−352.

(20) Sun, N.; Liu, Y.; Qin, L.; Lee, H.; Weissleder, R.; Ham, D. *Solid-State Electron.* **2013**, *84*, 13−21.

(21) Ha, D.; Paulsen, J.; Sun, N.; Song, Y. Q.; Ham, D. *Proc. Natl. Acad. Sci. U. S. A.* **2014**, *111* (33), 11955−11960.

(22) Ha, D.; Sun, N.; Ham, D. *eMagRes.* **2015**, *4* (1), 117−125.

(23) Li, Y.; Wolters, A. M.; Malawey, P. V.; Sweedler, J. V.; Webb, A. G. *Anal. Chem.* **1999**, *71* (21), 4815−4820.

(24) Norcross, J. A.; Milling, C. T.; Olson, D. L.; Xu, D.; Audrieth, A.; Albrecht, R.; Ruan, K.; Likos, J.; Jones, C.; Peck, T. L. *Anal. Chem.* **2010**, *82* (17), 7227−7236.

(25) Wang, H.; Ciobanu, L.; Webb, A. *J. Magn. Reson.* **2005**, *173* (1), 134−139.

(26) Högemann, D.; Ntziachristos, V.; Josephson, L.; Weissleder, R. *Bioconjugate Chem.* **2002**, *13* (1), 116−121.

(27) Macnaughtan, M. A.; Hou, T.; Xu, J.; Raftery, D. *Anal. Chem.* **2003**, *75* (19), 5116−5123.

(28) Huber, S.; Min, C.; Staat, C.; Oh, J.; Castro, C. M.; Haase, A.; Weissleder, R.; Gleich, B.; Lee, H. *Biosens. Bioelectron.* **2019**, *126*, 240−248.

(29) Anderson, W. A. *Rev. Sci. Instrum.* **1961**, *32* (3), 241−250.

(30) Bloch, F. *Phys. Rev.* **1954**, *94* (2), 496−497.

(31) Anderson, W. A.; Arnold, J. T. *Phys. Rev.* **1954**, *94* (2), 497−498.

(32) Hürlimann, M. D.; Venkataramanan, L. *J. Magn. Reson.* **2002**, *157* (1), 31−42.

(33) Hürlimann, M. D.; Venkataramanan, L.; Flaum, C.; Speier, P.; Karmonik, C.; Freedman, R.; Heaton, N. *SPWLA 43rd Annual Logging Symp.* **2002**, 1−14.

(34) Hürlimann, M. D.; Burcaw, L.; Song, Y.-Q. *J. Colloid Interface Sci.* **2006**, *297* (1), 303−311.

(35) Flaum, M.; Chen, J.; Hirasaki, G. J. *Petrophysics* **2005**, *46* (2), 113−123.

(36) Taktak, S.; Sosnovik, D.; Cima, M. J.; Weissleder, R.; Josephson, L. *Anal. Chem.* **2007**, *79* (23), 8863−8869.

(37) Perez, J. M.; Josephson, L.; O'Loughlin, T.; Högemann, D.; Weissleder, R. *Nat. Biotechnol.* **2002**, *20* (8), 816−820.

(38) Lee, H.; Sun, E.; Ham, D.; Weissleder, R. *Nat. Med.* **2008**, *14* (8), 869−874.

DOI: 10.1021/acs.analchem.9b04633
Anal. Chem. 2020, 92, 2112−2120

(39) Hennig, J.; Nauerth, A.; Friedburg, H. *Magn. Reson. Med.* **1986**, *3* (6), 823−833.
(40) Feinberg, D. A.; Hale, J. D.; Watts, J. C.; Kaufman, L.; Mark, A. *Radiology* **1986**, *161* (2), 527−531.
(41) Indrawati, L.; Stroshine, R. L.; Narsimhan, G. *J. Sci. Food Agric.* **2007**, *87* (12), 2207−2216.
(42) Hills, B. P.; Takacs, S. F.; Belton, P. S. *Mol. Phys.* **1989**, *67* (4), 919−937.
(43) Pascone, R.; Vullo, T.; Cahill, P. T.; Tankhiwale, A. *Nucl. Sci. Symp. Med. Imaging Conf.* **1993**, 1349−1353.
(44) Yutzy, S. R.; Seiberlich, N.; Duerk, J. L.; Griswold, M. A. *Magn. Reson. Med.* **2011**, *65* (6), 1630−1637.
(45) Larkman, D. J.; Nunes, R. G. *Phys. Med. Biol.* **2007**, *52* (7), R15−R55.

DOI: 10.1021/acs.analchem.9b04633
Anal. Chem. 2020, 92, 2112−2120